Revisiting lepton-specific 2HDM in light of muon $g - 2$ anomaly

Lei Wang [a,*], Jin Min Yang [b,c,d], Mengchao Zhang [e], Yang Zhang [f]

[a] *Department of Physics, Yantai University, Yantai 264005, China*
[b] *CAS Key Laboratory of Theoretical Physics, Institute of Theoretical Physics, Chinese Academy of Sciences, Beijing 100190, China*
[c] *School of Physical Sciences, University of Chinese Academy of Sciences, Beijing 100049, China*
[d] *Department of Physics, Tohoku University, Sendai 980-8578, Japan*
[e] *Center for Theoretical Physics of the Universe, Institute for Basic Science (IBS), Daejeon, 34126, Korea*
[f] *ARC Centre of Excellence for Particle Physics at the Tera-scale, School of Physics and Astronomy, Monash University, Melbourne, Victoria 3800, Australia*

A R T I C L E   I N F O

A B S T R A C T

We examine the lepton-specific 2HDM as a solution of muon $g - 2$ anomaly under various theoretical and experimental constraints, especially the direct search limits from the LHC and the requirement of a strong first-order phase transition in the early universe. We find that the muon $g - 2$ anomaly can be explained in the region of $32 < \tan\beta < 80$, 10 GeV $< m_A < 65$ GeV, 260 GeV $< m_H < 620$ GeV and 180 GeV $< m_{H^\pm} < 620$ GeV after imposing the joint constraints from the theory, the precision electroweak data, the 125 GeV Higgs data, the leptonic/semi-hadronic τ decays, the leptonic Z decays and Br($B_s \to \mu^+\mu^-$). The direct searches from the $h \to AA$ channels can impose stringent upper limits on Br($h \to AA$) and the multi-lepton event searches can sizably reduce the allowed region of m_A and $\tan\beta$ (10 GeV $< m_A <$ 44 GeV and $32 < \tan\beta < 60$). Finally, we find that the model can produce a strong first-order phase transition in the region of 14 GeV $< m_A < 25$ GeV, 310 GeV $< m_H < 355$ GeV and 250 GeV $< m_{H^\pm} <$ 295 GeV, allowed by the explanation of the muon $g - 2$ anomaly.

© 2018 The Authors. Published by Elsevier B.V. This is an open access article under the CC BY license (http://creativecommons.org/licenses/by/4.0/). Funded by SCOAP³.

1. Introduction

The muon anomalous magnetic moment $(g - 2)$ is a very precisely measured observable. The muon $g - 2$ anomaly has been a long-standing puzzle since the announcement by the E821 experiment in 2001 [1,2]. The experimental value has an approximate 3σ discrepancy from the SM prediction [3–5]. As a popular extension of the SM, the two Higgs doublet models (2HDM) have been applied to explain the muon $g - 2$ anomaly in the literature [6–31]. Among these extensions, the lepton-specific 2HDM (L2HDM) provides a simple explanation for the muon $g - 2$ anomaly [11,14–17, 22]. A light pseudoscalar with a large coupling to lepton can sizably enhance the muon $g - 2$ via the two-loop Barr–Zee diagrams.

In this work we examine the parameter space of L2HDM by considering the joint constraints from the theory, the precision electroweak data, the 125 GeV Higgs signal data, the muon $g - 2$ anomaly, the lepton flavor universality (LFU) in the τ and Z decays, the measurement of Br($B_s \to \mu^+\mu^-$), as well as the direct search limits from the LHC (the data of some channels analyzed by the ATLAS and CMS are corresponding to an integrated lumi-

nosity up to about 36 fb^{-1} recorded in proton–proton collisions at $\sqrt{s} = 13$ TeV). On the other hand, it is known that the 2HDM can trigger a strong first-order phase transition (SFOPT) in the early universe [32,33], which is required by a successful explanation of the observed baryon asymmetry of the universe (BAU) [34] and can produce primordial gravitational-wave (GW) signals [35] potentially detectable by future space-based laser interferometer detectors like eLISA [36]. Due to the importance of SFOPT in cosmology, we will also analyze whether a SFOPT is achievable in the parameter space in favor of the muon $g - 2$ explanation.

Our work is organized as follows. In Sec. 2 we recapitulate the L2HDM. In Sec. 3 we discuss the muon $g - 2$ anomaly and other relevant constraints. In Sec. 4, we constrain the model using the direct search limits from the LHC. In Sec. 5, we discuss some benchmark scenarios leading to a SFOPT. Finally, we give our conclusion in Sec. 6.

2. The lepton-specific 2HDM

The Higgs potential with a softly-broken discrete Z_2 symmetry is given as [37]

$$V = m_{11}^2(\Phi_1^\dagger\Phi_1) + m_{22}^2(\Phi_2^\dagger\Phi_2) - \left[m_{12}^2(\Phi_1^\dagger\Phi_2 + \text{h.c.})\right]$$

* Corresponding author.
E-mail address: leiwang@ytu.edu.cn (L. Wang).

$$+ \frac{\lambda_1}{2}(\Phi_1^\dagger \Phi_1)^2 + \frac{\lambda_2}{2}(\Phi_2^\dagger \Phi_2)^2 + \lambda_3(\Phi_1^\dagger \Phi_1)(\Phi_2^\dagger \Phi_2)$$

$$+ \lambda_4(\Phi_1^\dagger \Phi_2)(\Phi_2^\dagger \Phi_1) + \left[\frac{\lambda_5}{2}(\Phi_1^\dagger \Phi_2)^2 + \text{h.c.} \right]. \tag{1}$$

In this paper we focus on the CP-conserving case where all λ_i and m_{12}^2 are real. The two complex scalar doublets respectively have the vacuum expectation values (VEVs) v_1 and v_2 with $v^2 = v_1^2 + v_2^2 = (246 \text{ GeV})^2$, and the ratio of the two VEVs is defined as usual to be $\tan\beta = v_2/v_1$. There are five mass eigenstates: two neutral CP-even states h and H, one neutral pseudoscalar A, and two charged scalars $H^\pm$.

In the L2HDM, the quarks obtain masses from Φ_2 field, and the leptons from Φ_1 field [38,39]. The Yukawa interactions are given by

$$-\mathcal{L} = Y_{u2} \, \overline{Q}_L \, \tilde{\Phi}_2 \, u_R + Y_{d2} \, \overline{Q}_L \, \Phi_2 \, d_R + Y_{\ell 1} \, \overline{L}_L \, \Phi_1 \, e_R + \text{h.c.}, \tag{2}$$

where $Q_L^T = (u_L, d_L)$, $L_L^T = (\nu_L, l_L)$, $\tilde{\Phi}_{1,2} = i\tau_2 \Phi_{1,2}^*$, and Y_{u2}, Y_{d2} and $Y_{\ell 1}$ are 3×3 matrices in family space.

The Yukawa couplings of the neutral Higgs bosons normalized to the SM are given by

$$y_V^h = \sin(\beta-\alpha), \quad y_f^h = [\sin(\beta-\alpha) + \cos(\beta-\alpha)\kappa_f],$$

$$y_V^H = \cos(\beta-\alpha), \quad y_f^H = [\cos(\beta-\alpha) - \sin(\beta-\alpha)\kappa_f],$$

$$y_V^A = 0, \quad y_A^f = -i\kappa_f \,(\text{for } u), \quad y_f^A = i\kappa_f \,(\text{for } d, \ell), \tag{3}$$

where V denotes Z or W, $\kappa_\ell \equiv -\tan\beta$, $\kappa_d = \kappa_u \equiv 1/\tan\beta$ and α is the mixing angle of the two CP-even Higgs bosons.

3. Muon $g-2$ anomaly and relevant constraints

3.1. Numerical calculations

In this paper, the light CP-even Higgs h is taken as the SM-like Higgs, $m_h = 125$ GeV. We take a convention [40], $0 \leq \beta \leq \frac{\pi}{2}$ and $-\frac{\pi}{2} \leq \beta - \alpha \leq \frac{\pi}{2}$, which leads to $0 \leq \cos(\beta-\alpha) \leq 1$ and $-1 \leq \sin(\beta-\alpha) \leq 1$. We take $\tan\beta$ and $\sin(\beta-\alpha)$ as input parameters, which replace the mixing angles β and α, respectively. If $\sin(\beta-\alpha)$ and $\tan\beta$ are given, we can determine β and α by $\beta = \arctan\beta$ and $\alpha = \arctan\beta - \arcsin(\beta-\alpha)$, respectively. Since the muon $g-2$ anomaly favors a light pseudoscalar with a large coupling to lepton, we scan over m_A and $\tan\beta$ in the following ranges:

$$10 \text{ GeV} < m_A < 120 \text{ GeV}, \quad 20 < \tan\beta < 120. \tag{4}$$

Such $\tan\beta$ can make $|y_f^h|$ to deviate from 1 sizably for a large $\cos(\beta-\alpha)$, which is disfavored by the signal data of the 125 GeV Higgs. Therefore, we take $|\sin(\beta-\alpha)|$ to be close to 1. According to the results on $\sin(\beta-\alpha)$ in Ref. [15], we scan over $\sin(\beta-\alpha)$ in the following ranges:

$$0.994 \leq \sin(\beta-\alpha) \leq 1, \quad -1 \leq \sin(\beta-\alpha) \leq -0.994. \tag{5}$$

In our calculation, we consider the following observables and constraints:

(1) Theoretical constraints and precision electroweak data. The 2HDMC [40] is employed to implement the theoretical constraints from the vacuum stability, unitarity and coupling-constant perturbativity, as well as the constraints from the oblique parameters (S, T, U).

(2) The signal data of the 125 GeV Higgs. Since the 125 GeV Higgs couplings with the SM particles in this model can deviate from the SM ones, the SM-like decay modes will be modified. Besides, for m_A is smaller than 62.5 GeV, the invisible decay $h \to AA$ is kinematically allowed, which will be strongly constrained by the experimental data of the 125 GeV Higgs. We perform χ_h^2 calculation for the signal strengths of the 125 GeV Higgs in the $\mu_{ggF+tth}(Y)$ and $\mu_{VBF+Vh}(Y)$ with Y denoting the decay mode $\gamma\gamma$, ZZ, WW, $\tau^+\tau^-$ and $b\bar{b}$,

$$\chi^2(Y) = \begin{pmatrix} \mu_{ggH+ttH}(Y) - \widehat{\mu}_{ggH+ttH}(Y) \\ \mu_{VBF+VH}(Y) - \widehat{\mu}_{VBF+VH}(Y) \end{pmatrix}^T \begin{pmatrix} a_Y & b_Y \\ b_Y & c_Y \end{pmatrix}$$
$$\times \begin{pmatrix} \mu_{ggH+ttH}(Y) - \widehat{\mu}_{ggH+ttH}(Y) \\ \mu_{VBF+VH}(Y) - \widehat{\mu}_{VBF+VH}(Y) \end{pmatrix}, \tag{6}$$

where $\widehat{\mu}_{ggH+ttH}(Y)$ and $\widehat{\mu}_{VBF+VH}(Y)$ are the data best-fit values and a_Y, b_Y and c_Y are the parameters of the ellipse, which are given by the combined ATLAS and CMS experiments [41].

(3) LFU in the τ decays. The HFAG collaboration reported three ratios from pure leptonic processes, and two ratios from semi-hadronic processes, $\tau \to \pi/K\nu$ and $\pi/K \to \mu\nu$ [42]:

$$\left(\frac{g_\tau}{g_\mu}\right) = 1.0011 \pm 0.0015, \quad \left(\frac{g_\tau}{g_e}\right) = 1.0029 \pm 0.0015,$$

$$\left(\frac{g_\mu}{g_e}\right) = 1.0018 \pm 0.0014, \quad \left(\frac{g_\tau}{g_\mu}\right)_\pi = 0.9963 \pm 0.0027,$$

$$\left(\frac{g_\tau}{g_\mu}\right)_K = 0.9858 \pm 0.0071. \tag{7}$$

The correlation matrix for the above five observables is

$$\begin{pmatrix} 1 & +0.53 & -0.49 & +0.24 & +0.12 \\ +0.53 & 1 & +0.48 & +0.26 & +0.10 \\ -0.49 & +0.48 & 1 & +0.02 & -0.02 \\ +0.24 & +0.26 & +0.02 & 1 & +0.05 \\ +0.12 & +0.10 & -0.02 & +0.05 & 1 \end{pmatrix}. \tag{8}$$

In the L2HDM we have the ratios

$$\left(\frac{g_\tau}{g_\mu}\right) \approx 1 + \delta_{\text{loop}}, \quad \left(\frac{g_\tau}{g_e}\right) \approx 1 + \delta_{\text{tree}} + \delta_{\text{loop}},$$

$$\left(\frac{g_\mu}{g_e}\right) \approx 1 + \delta_{\text{tree}}, \quad \left(\frac{g_\tau}{g_\mu}\right)_\pi \approx 1 + \delta_{\text{loop}},$$

$$\left(\frac{g_\tau}{g_\mu}\right)_K \approx 1 + \delta_{\text{loop}}, \tag{9}$$

where δ_{tree} and δ_{loop} are respectively corrections from the tree-level diagrams and the one-loop diagrams mediated by the charged Higgs. They are given as [16,22]

$$\delta_{\text{tree}} = \frac{m_\tau^2 m_\mu^2}{8 m_{H^\pm}^4} t_\beta^4 - \frac{m_\mu^2}{m_{H^\pm}^2} t_\beta^2 \frac{g(m_\mu^2/m_\tau^2)}{f(m_\mu^2/m_\tau^2)}, \tag{10}$$

$$\delta_{\text{loop}} = \frac{1}{16\pi^2} \frac{m_\tau^2}{v^2} t_\beta^2 \left[1 + \frac{1}{4}\Big(H(x_A) + s_{\beta-\alpha}^2 H(x_H) + c_{\beta-\alpha}^2 H(x_h) \Big) \right], \tag{11}$$

where $f(x) \equiv 1 - 8x + 8x^3 - x^4 - 12x^2 \ln(x)$, $g(x) \equiv 1 + 9x - 9x^2 - x^3 + 6x(1+x)\ln(x)$ and $H(x_\phi) \equiv \ln(x_\phi)(1+x_\phi)/(1-x_\phi)$ with $x_\phi = m_\phi^2/m_{H^\pm}^2$.

We perform χ_τ^2 calculation for the five observables. The covariance matrix constructed from the data of Eq. (7) and Eq. (8) has a vanishing eigenvalue, and the corresponding degree is removed in our calculation.

(4) LFU in the Z decays. The measured values of the ratios of the leptonic Z decay branching fractions are given as [43]:

$$\frac{\Gamma_{Z\to\mu^+\mu^-}}{\Gamma_{Z\to e^+e^-}} = 1.0009 \pm 0.0028\,, \tag{12}$$

$$\frac{\Gamma_{Z\to\tau^+\tau^-}}{\Gamma_{Z\to e^+e^-}} = 1.0019 \pm 0.0032\,, \tag{13}$$

with a correlation of $+0.63$. In the L2HDM, the width of $Z \to \tau^+\tau^-$ can have sizable deviation from the SM value by the loop contributions of the extra Higgs bosons, because they strongly interact with charged leptons for large $\tan\beta$. The quantities of Eq. (12) are calculated in the L2HDM as [16,22]

$$\frac{\Gamma_{Z\to\mu^+\mu^-}}{\Gamma_{Z\to e^+e^-}} \approx 1.0 + \frac{2g_L^e\,\mathrm{Re}(\delta g_L^{\mathrm{2HDM}}) + 2g_R^e\,\mathrm{Re}(\delta g_R^{\mathrm{2HDM}})}{g_L^{e\,2}+g_R^{e\,2}}\frac{m_\mu^2}{m_\tau^2}\,, \tag{14}$$

$$\frac{\Gamma_{Z\to\tau^+\tau^-}}{\Gamma_{Z\to e^+e^-}} \approx 1.0 + \frac{2g_L^e\,\mathrm{Re}(\delta g_L^{\mathrm{2HDM}}) + 2g_R^e\,\mathrm{Re}(\delta g_R^{\mathrm{2HDM}})}{g_L^{e\,2}+g_R^{e\,2}}\,, \tag{15}$$

where the SM value $g_L^e = -0.27$ and $g_R^e = 0.23$. $\delta g_L^{\mathrm{2HDM}}$ and $\delta g_R^{\mathrm{2HDM}}$ are from the one-loop corrections of L2HDM, which are explicitly given in Ref. [22].

(5) The muon $g-2$. The recent measurement is $a_\mu^{exp} = (116592091 \pm 63) \times 10^{-11}$ [44], which has approximately 3.1σ deviation from the SM prediction [45], $\Delta a_\mu = a_\mu^{exp} - a_\mu^{SM} = (262 \pm 85) \times 10^{-11}$. In this paper, we require the model to explain the muon $g-2$ anomaly at the 2σ level.

In the L2HDM, the muon $g-2$ obtains contributions from the one-loop diagrams induced by the Higgs bosons and also from the two-loop Barr–Zee diagrams mediated by A, h and H. For the one-loop contributions [6] we have

$$\Delta a_\mu^{\mathrm{2HDM}}(1\mathrm{loop}) = \frac{G_F m_\mu^2}{4\pi^2\sqrt{2}}\sum_j\left(y_\mu^j\right)^2 r_\mu^j\, f_j(r_\mu^j)\,, \tag{16}$$

where $j = h, H, A, H^\pm$, $r_\mu^j = m_\mu^2/M_j^2$. For $r_\mu^j \ll 1$ we have

$$f_{h,H}(r) \simeq -\ln r - 7/6,\quad f_A(r) \simeq \ln r + 11/6,$$
$$f_{H^\pm}(r) \simeq -1/6. \tag{17}$$

The two-loop contributions are given by

$$\Delta a_\mu^{\mathrm{2HDM}}(2\mathrm{loop-BZ})$$
$$= \frac{G_F m_\mu^2}{4\pi^2\sqrt{2}}\frac{\alpha_{\mathrm{em}}}{\pi}\sum_{i,f} N_f^c\, Q_f^2\, y_\mu^i\, y_f^i\, r_f^i\, g_i(r_f^i)\,, \tag{18}$$

where $i = h, H, A$, and m_f, Q_f and N_f^c are the mass, electric charge and the number of color degrees of freedom of the fermion f in the loop. The functions $g_i(r)$ are [7,8,10]

$$g_{h,H}(r) = \int_0^1 dx\,\frac{2x(1-x)-1}{x(1-x)-r}\ln\frac{x(1-x)}{r}\,, \tag{19}$$

$$g_A(r) = \int_0^1 dx\,\frac{1}{x(1-x)-r}\ln\frac{x(1-x)}{r}\,. \tag{20}$$

The contributions of the CP-even (CP-odd) Higgses to a_μ are negative (positive) at the two-loop level and positive (negative) at one-loop level. As m_f^2/m_μ^2 could easily overcome the

loop suppression factor α/π, the two-loop contributions can be larger than one-loop ones.

(6) $B_s \to \mu^+\mu^-$. We take the formulas in [46] to calculate $B_s \to \mu^+\mu^-$

$$\frac{\overline{\mathcal{B}}(B_s \to \mu^+\mu^-)}{\overline{\mathcal{B}}(B_s \to \mu^+\mu^-)_{\mathrm{SM}}} = \left[|P|^2 + \left(1 - \frac{\Delta\Gamma_s}{\Gamma_L^s}\right)|S|^2\right], \tag{21}$$

where the CKM matrix elements and hadronic factors cancel out, and

$$P \equiv \frac{C_{10}}{C_{10}^{\mathrm{SM}}} + \frac{M_{B_s}^2}{2M_W^2}\left(\frac{m_b}{m_b+m_s}\right)\frac{C_P - C_P^{\mathrm{SM}}}{C_{10}^{\mathrm{SM}}}\,, \tag{22}$$

$$S \equiv \sqrt{1 - \frac{4m_\mu^2}{M_{B_s}^2}}\,\frac{M_{B_s}^2}{2M_W^2}\left(\frac{m_b}{m_b+m_s}\right)\frac{C_S - C_S^{\mathrm{SM}}}{C_{10}^{\mathrm{SM}}}\,. \tag{23}$$

The L2HDM can give the additional contributions to coefficient C_{10} by the Z-penguin diagrams with the charged Higgs loop. Unless there are large enhancements for C_P and C_S, their contributions can be neglected due to the suppression of the factor $M_{B_s}^2/M_W^2$. In the L2HDM, C_P can obtain the important contributions from the CP-odd Higgs exchange diagrams for a very small m_A. The experimental data of $\mathrm{Br}(B_s \to \mu\mu)$ is given as [47]

$$\mathrm{Br}(B_s \to \mu\mu) = (3.0 \pm 0.6^{+0.3}_{-0.2}) \times 10^{-9}\,. \tag{24}$$

(7) The exclusion limits from the searches for Higgs bosons at the LEP and $h \to AA$ at the LHC. We employ HiggsBounds [50,51] to implement the exclusion constraints from the searches for the neutral and charged Higgs at the LEP at 95% confidence level. The searches for a light Higgs at the LEP can impose stringent constraints on the parameter space.

The ATLAS and CMS have searched for some exotic decay channels of the 125 GeV Higgs, such as $h \to AA$. In addition to the global fit to the 125 GeV Higgs signal data, the hAA coupling will be constrained by the ATLAS and CMS direct searches for $h \to AA$ channels at the LHC. Table 1 shows several $h \to AA$ channels considered by us.

The 125 GeV Higgs signal data and the LFU data from τ decays include a large number of observables. We perform a global fit to the 125 GeV Higgs signal data and the LFU data from τ decays, and define χ^2 as $\chi^2 = \chi_h^2 + \chi_\tau^2$. We pay particular attention to the surviving samples with $\chi^2 - \chi_{\min}^2 \le 6.18$, where $\chi_{\min}^2$ denotes the minimum of χ^2. These samples correspond to be within the 2σ range in any two-dimension plane of the model parameters when explaining the signal data of the 125 GeV Higgs and the data of the LFU from τ decays.

3.2. Results and discussions

In Fig. 1, we project the surviving samples within 1σ, 2σ, and 3σ ranges of $\Delta\chi^2$ on the planes of $\tan\beta$ VS m_A, $\tan\beta$ VS $m_{H^\pm}$, and m_A VS $m_{H^\pm}$ after imposing the constraints from theory, the oblique parameters, the exclusion limits from searches for Higgs at LEP, the signal data of the 125 GeV Higgs, and the LFU in τ decays. We obtain a surviving sample with a minimal value of χ^2 fit to the 125 GeV Higgs signal data and the LFU data in τ decays, $\chi_{min}^2 = 16.99$. The upper-left panel of Fig. 1 shows that the value of χ^2 is favored to increase with $\tan\beta$ and with a decrease of $m_{H^\pm}$. This is because the LFU in τ decays is significantly corrected by the tree-level diagrams mediated by the

Table 1
The upper limits at 95% C.L. on the production cross-section times branching ratio for $h \to AA$ channels at the LHC.

| Channel	Experiment	Mass range (GeV)	Luminosity
$gg \to h \to AA \to \tau^+\tau^-\tau^+\tau^-$	ATLAS 8 TeV [48]	4–50	20.3 fb^{-1}
$pp \to h \to AA \to \tau^+\tau^-\tau^+\tau^-$	CMS 8 TeV [49]	5–15	19.7 fb^{-1}
$pp \to h \to AA \to (\mu^+\mu^-)(b\bar{b})$	CMS 8 TeV [49]	25–62.5	19.7 fb^{-1}
$pp \to h \to AA \to (\mu^+\mu^-)(\tau^+\tau^-)$	CMS 8 TeV [49]	15–62.5	19.7 fb^{-1}
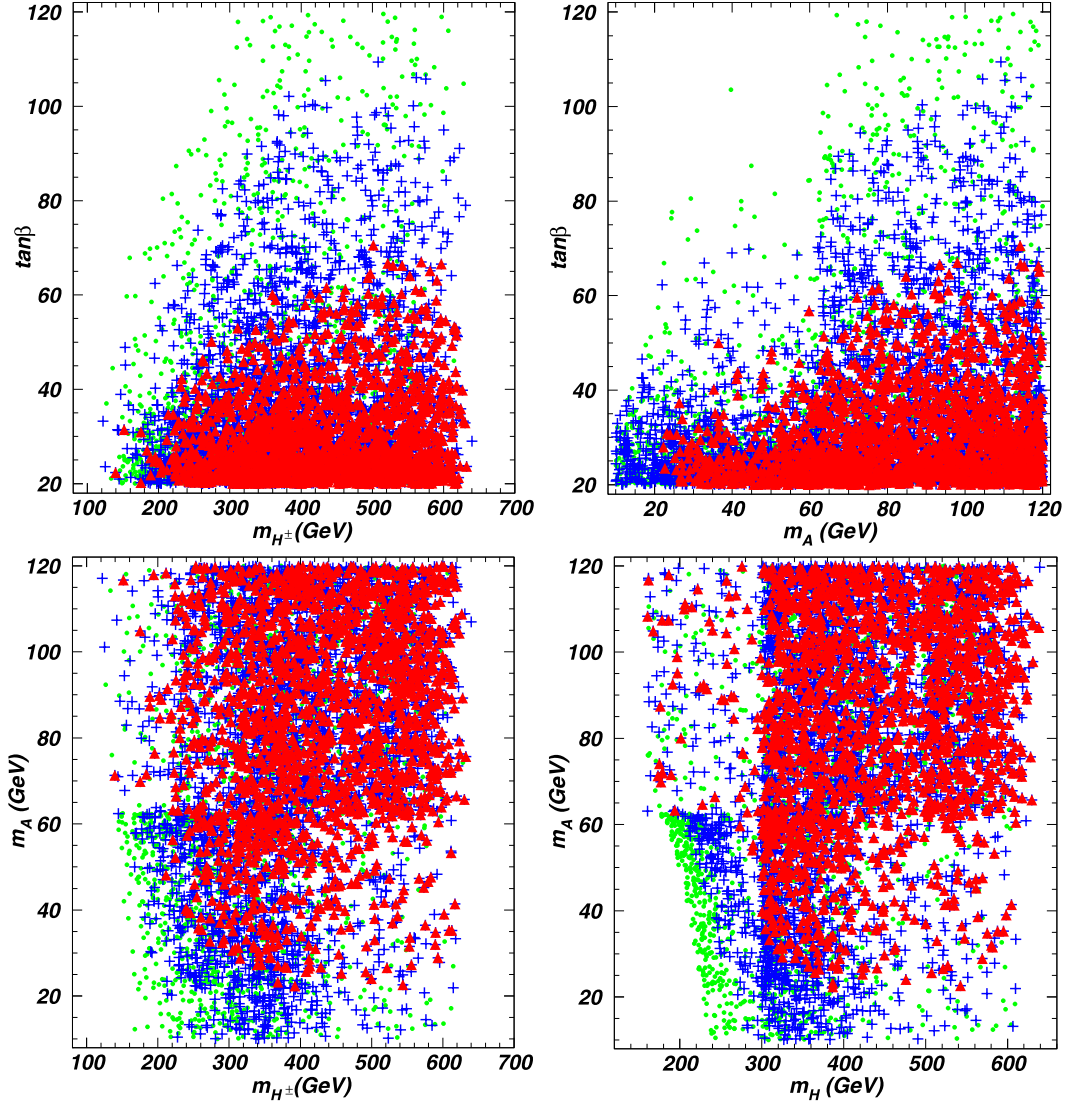
Fig. 1. The samples within the 1σ, 2σ and 3σ ranges of $\Delta\chi^2$ projected on the planes of $\tan\beta$ versus (VS) $m_{H^\pm}$, $\tan\beta$ VS m_A, m_A VS $m_{H^\pm}$, and m_A VS m_H after imposing the constraints from theory, the oblique parameters, the exclusion limits from searches for Higgs at LEP, the signal data of the 125 GeV Higgs, and the LFU from the τ decays. The bullets (green), pluses (royal blue), and triangles (red) are respectively within the 3σ, 2σ and 1σ regions of $\Delta\chi^2$.

charged Higgs. The lower-left panel of Fig. 1 shows that χ^2 is favored to have a large value for a small m_A. For $m_A < m_{H^\pm}$, the large mass splitting between m_A and $m_{H^\pm}$ can make the one-loop diagram to give sizable correction to the LFU in τ decays. The upper-right panel shows that, for a light pseudoscalar, such as $m_A < 25$ GeV, $\tan\beta$ is strongly imposed an upper limit. The main constraints are from the exclusion limits from the searches for Higgs at LEP. Ref. [26] also obtained the limits from LEP on $\tan\beta$ for $m_A < 25$ GeV. Our results are consistent with those of Ref. [26], such as $\tan\beta > 35$ (60) for m_A around 10 GeV (20 GeV). Most of regions of $m_A < 60$ GeV and $m_H < 300$ GeV are beyond the 2σ range of $\Delta\chi^2$, as shown in lower-right panel of Fig. 1. The

main constraints are from the signal data of the 125 GeV Higgs and the theory.

The left panel of Fig. 2 shows that $\sin(\beta - \alpha)$ and $\tan\beta$ are restricted to be a narrow region. From the Eq. (3), the τ Yukawa coupling of the 125 GeV Higgs normalized to the SM is $y_\tau^h = \sin(\beta - \alpha) - \cos(\beta - \alpha)\tan\beta$ with $\cos(\beta - \alpha) > 0$, and $| y_\tau^h |$ can significantly deviate from 1.0 for a large $\tan\beta$, which is disfavored by the signal data of the 125 GeV Higgs. Therefore, an appropriate $\sin(\beta - \alpha)$ is required to make $| y_\tau^h |$ to be around 1.0. A simple solution is $|\sin(\beta - \alpha)|$ very close to 1.0. However, the constraints of theory and Br($h \to AA$) < 0.3 require $\tan\beta < 10$, and the detailed discussions are given in Ref. [52] (see Fig. 1 of Ref. [52]). Therefore,
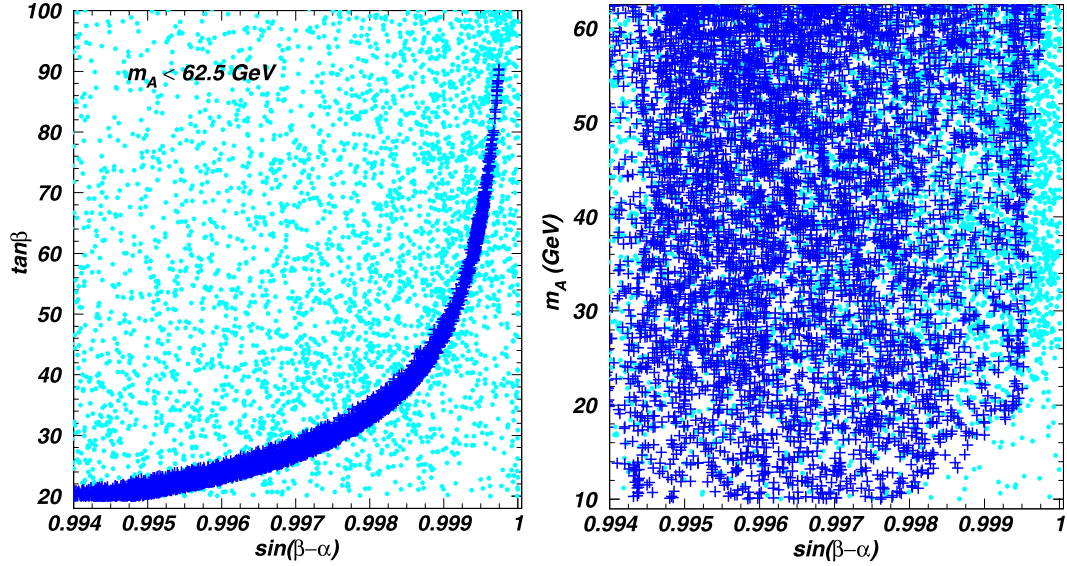
Fig. 2. The surviving samples projected on the planes of $\sin(\beta - \alpha)$ VS $\tan\beta$ and $\sin(\beta - \alpha)$ VS m_A. The bullets (sky blue) and pluses (royal blue) are allowed by the constraints from theory, the oblique parameters, the exclusion limits from searches for Higgses at LEP. In addition, the pluses (royal blue) are within the 2σ regions of $\triangle\chi^2$.
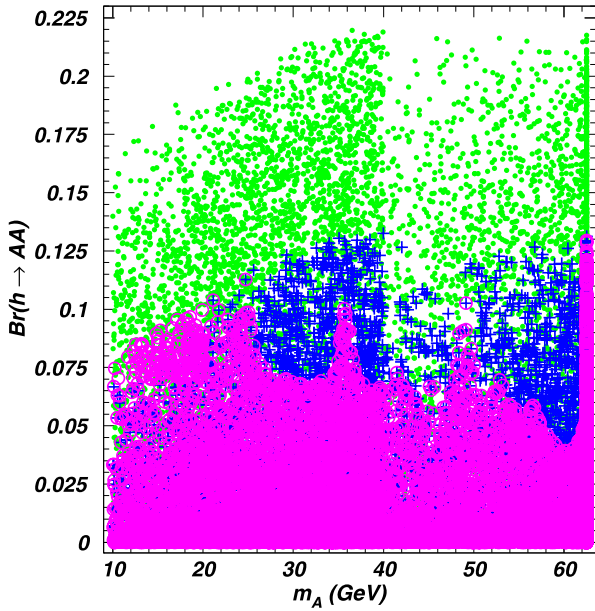
Fig. 3. The surviving samples on the planes of $Br(h \to AA)$ VS m_A after imposing the constraints from "pre-muon $g - 2$". The bullets (green) and crosses (blue) are respectively within the 3σ and 2σ regions of $\triangle\chi^2$. The circles (pink) are within the 2σ regions of $\triangle\chi^2$ and allowed by the exclusion limits from $h \to AA$ channels at the LHC.

such solution is excluded for $\tan\beta > 20$ in our paper, as shown in the right panel of Fig. 2. For $\sin(\beta - \alpha) > 0$, $|\sin(\beta - \alpha)|$ is allowed to deviate from 1.0 properly. The corresponding $-y_\tau^h$ is around 1.0, and y_τ^h is opposite in sign from the gauge boson coupling of the 125 GeV Higgs. This is so called the wrong sign Yukawa coupling of 125 GeV Higgs. For example, $y_\tau^h = -1.01$ for $\sin(\beta - \alpha) = 0.999$ and $\tan\beta = 45$. For $\sin(\beta - \alpha) < 0$, y_τ^h is smaller than 0, and its absolute value deviates from 1.0 significantly, which is excluded. In addition, for $m_A < 20$ GeV, the exclusion limits from the searches for Higgs at LEP impose an upper bound on $\tan\beta$. As a result, some large values of $\sin(\beta - \alpha)$ are excluded for $m_A < 20$ GeV according to the dependence of $\tan\beta$ on $\sin(\beta - \alpha)$ shown in the left panel.

In Fig. 3, we project the surviving samples on the planes of $Br(h \to AA)$ VS m_A after imposing the constraints from "pre-muon $g - 2$" (denoting the theory, the oblique parameters, the exclusion limits from the searches for Higgs at LEP, the signal data of the 125 GeV Higgs, the LFU in τ decays, and the exclusion limits from $h \to AA$ channels at LHC). The direct searches for $h \to AA$ channels at the LHC impose stringent upper limits on $Br(h \to AA)$ in the L2HDM, such as $Br(h \to AA) < 4\%$ for $m_A = 60$ GeV. Many samples within the 2σ range of $\triangle\chi^2$ are excluded.

In Fig. 4, we project the surviving samples on the planes of $\tan\beta$ VS m_A, $\tan\beta$ VS $m_{H^\pm}$, $\tan\beta$ VS m_H, m_A VS $m_{H^\pm}$, m_A VS m_H, and m_H VS $m_{H^\pm}$ after imposing the constraints from "pre-muon $g - 2$", muon $g - 2$ anomaly, the LFU in Z decays, and $Br(B_s \to \mu^+\mu^-)$. The lower-left and lower-middle panels show that the LFU in Z decays excludes most of samples in the large $m_{H^\pm}$ and m_H regions. This is because that the one-loop diagram can give sizable corrections to the LFU in Z decays for $m_A < m_{H^\pm}$ (m_H). The characteristic is also found in Refs. [12,22,26], and our results are consistent with theirs. Because of the constraints from the oblique parameters, H and $H^\pm$ are favored to have a small splitting mass for large $m_{H^\pm}$, as shown in the lower-right panel of Fig. 4. Ref. [14] also pointed out the constraints of $\triangle\rho$ on the mass splitting between H and $H^\pm$. The T parameter used in our paper is related to $\triangle\rho$. For $m_{H^\pm} < 250$ GeV, all the samples within 2σ region of $\triangle\chi^2$ are consistent with the limits of the LFU in Z decay. This is because the LFU in τ decays can give more stringent constraints on the L2HDM than the LFU in Z decays for a light charged Higgs.

The upper-left and lower-left panels of Fig. 4 show that the limits of $Br(B_s \to \mu^+\mu^-)$ exclude most of regions of m_A around 10 GeV and $m_{H^\pm} < 300$ GeV. The A exchange diagrams can give sizable contributions to $B_s \to \mu^+\mu^-$ for a very small m_A. In the L2HDM, the lepton couplings are enhanced by $\tan\beta$, while the quark couplings are suppressed by $\cot\beta$. Therefore, the leading contributions are almost independent on $\tan\beta$ for large $\tan\beta$.

Fig. 4 shows that with the limits from "pre-muon $g - 2$", the LFU in Z decays and $Br(B_s \to \mu^+\mu^-)$ being satisfied, the muon $g - 2$ anomaly can be explained in the regions of $32 < \tan\beta < 80$, 10 GeV $< m_A < 65$ GeV, 260 GeV $< m_H < 620$ GeV, and 180 GeV $< m_{H^\pm} < 620$ GeV. The upper-left panel of Fig. 4 shows that in the range of 65 GeV $< m_A < 100$ GeV, the muon $g - 2$ anomaly can
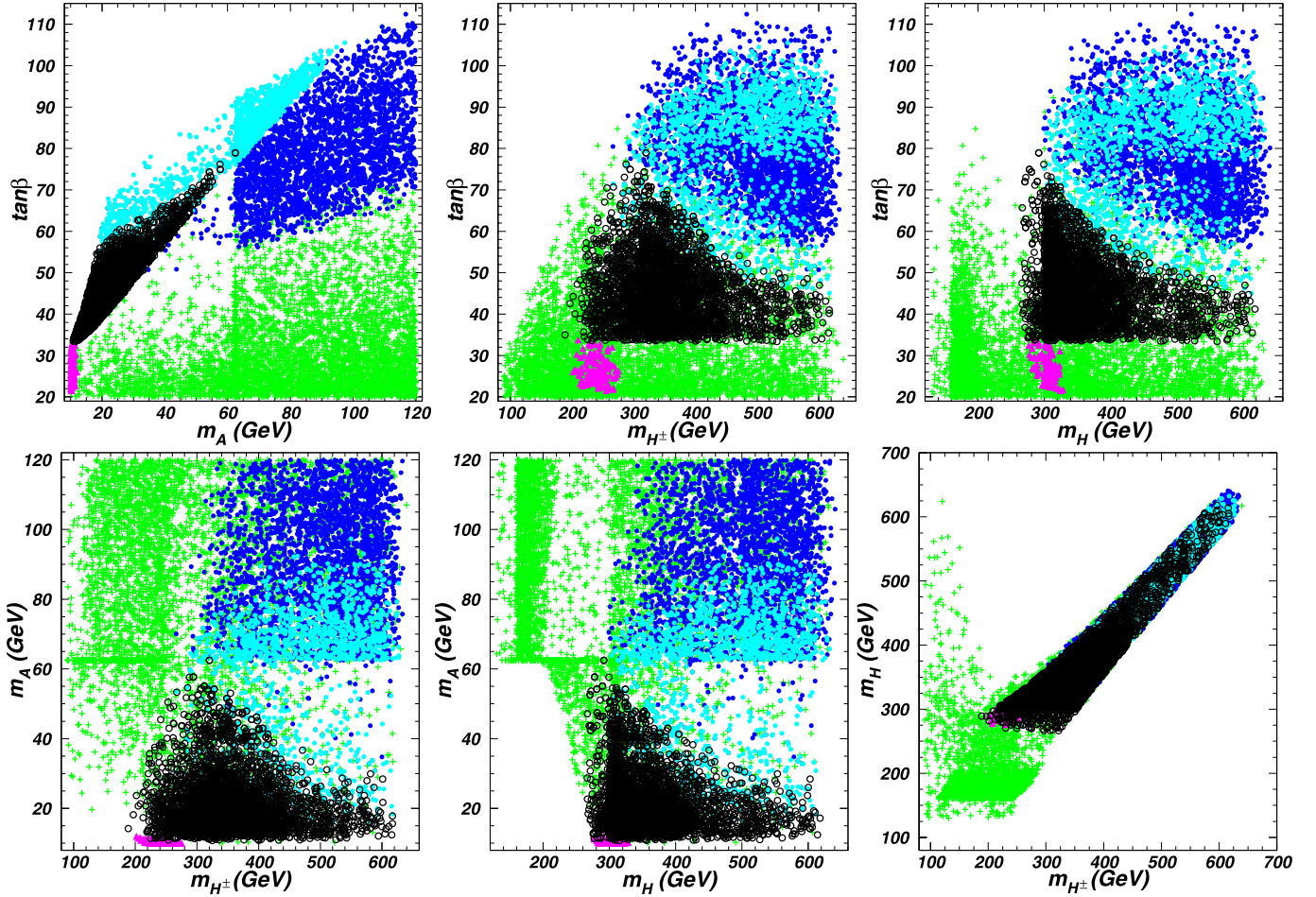
Fig. 4. The surviving samples projected on the planes of $\tan\beta$ VS m_A, $\tan\beta$ VS $m_{H^\pm}$, $\tan\beta$ VS m_H, m_A VS $m_{H^\pm}$, m_A VS m_H, and m_H VS $m_{H^\pm}$. The pluses (green) are allowed by the constraints of "pre-muon $g-2$". The triangles (pink) are allowed by the "pre-muon $g-2$", but excluded by the Br($B_s \to \mu^+\mu^-$) limits. The light bullets (sky blue) and dark bullets (royal blue) are allowed by the "pre-muon $g-2$", but excluded by the limits of the LFU in Z decay. In addition, the light bullets accommodate the muon $g-2$ anomaly and the dark bullets do not. The circles (black) are allowed by the constraints from the "pre-muon $g-2$", the LFU in Z decay, and Br($B_s \to \mu^+\mu^-$).

be explained for a large enough $\tan\beta$. However, such a large $\tan\beta$ is excluded by the LFU in Z decays. The contributions of A to the muon $g-2$ anomaly have destructive interference with those of H. Therefore, a large mass splitting between A and H is required to explain the muon $g-2$ anomaly, as shown in the lower-middle panel of Fig. 4.

Refs. [16,22,26] discussed the muon $g-2$ anomaly, the constraints from LFU in τ and Z decays in the L2HDM. Here we compare our results with those of Refs. [16,22,26]. Within the 2σ range of the muon $g-2$ anomaly, the dependence of $\tan\beta$ on m_A in our paper is almost consistent with those of Ref. [16] and Ref. [14]. However, Ref. [16] only considered the two ratios of $\frac{g_\tau}{g_e}$ and $\frac{g_\mu}{g_e}$ for the LFU in τ decay. As a result, the lower limits of $\tan\beta$ are more stringent than that of our paper. Within the 2σ range of the muon $g-2$ anomaly, the lower limits of $\tan\beta$ in Ref. [22] are smaller than those of Ref. [14] and our paper. Ref. [26] used the searches for A at the LEP, the experimental data of the LFU in τ and Z decays to restrict $\tan\beta$ and m_A, and took different approaches of considering these constraints. In this paper, we used the joint theoretical and experimental constraints, and $\tan\beta$ and m_A are stronger than those of Ref. [26]. Obviously, in our paper (see lower panels of Fig. 1) and Ref. [17] (see right panel of Fig. 2 and Fig. 5 in Ref. [17]), m_A below 50 GeV is excluded for $m_{H^\pm} = 150$ GeV and $m_H = 150$ GeV. However, such case is allowed in Fig. 1 of Ref. [26].

4. The direct search limits from the LHC

Here we discuss the direct search limits from the LHC. In the parameter space in favor of muon $g-2$ anomaly explanation, the production processes of extra Higgs bosons via the Yukawa interaction with quarks can be neglected due to the suppression of large $\tan\beta$ in the L2HDM. For m_A smaller than 62.5 GeV, a pair of pseudoscalars can be produced via $pp \to h \to AA$ at the LHC. In the above Section, we find that $h \to AA$ channel at the LHC can exclude many samples within the 2σ region of $\Delta\chi^2$.

The extra Higgs bosons are dominantly produced at the LHC via the following electroweak processes:
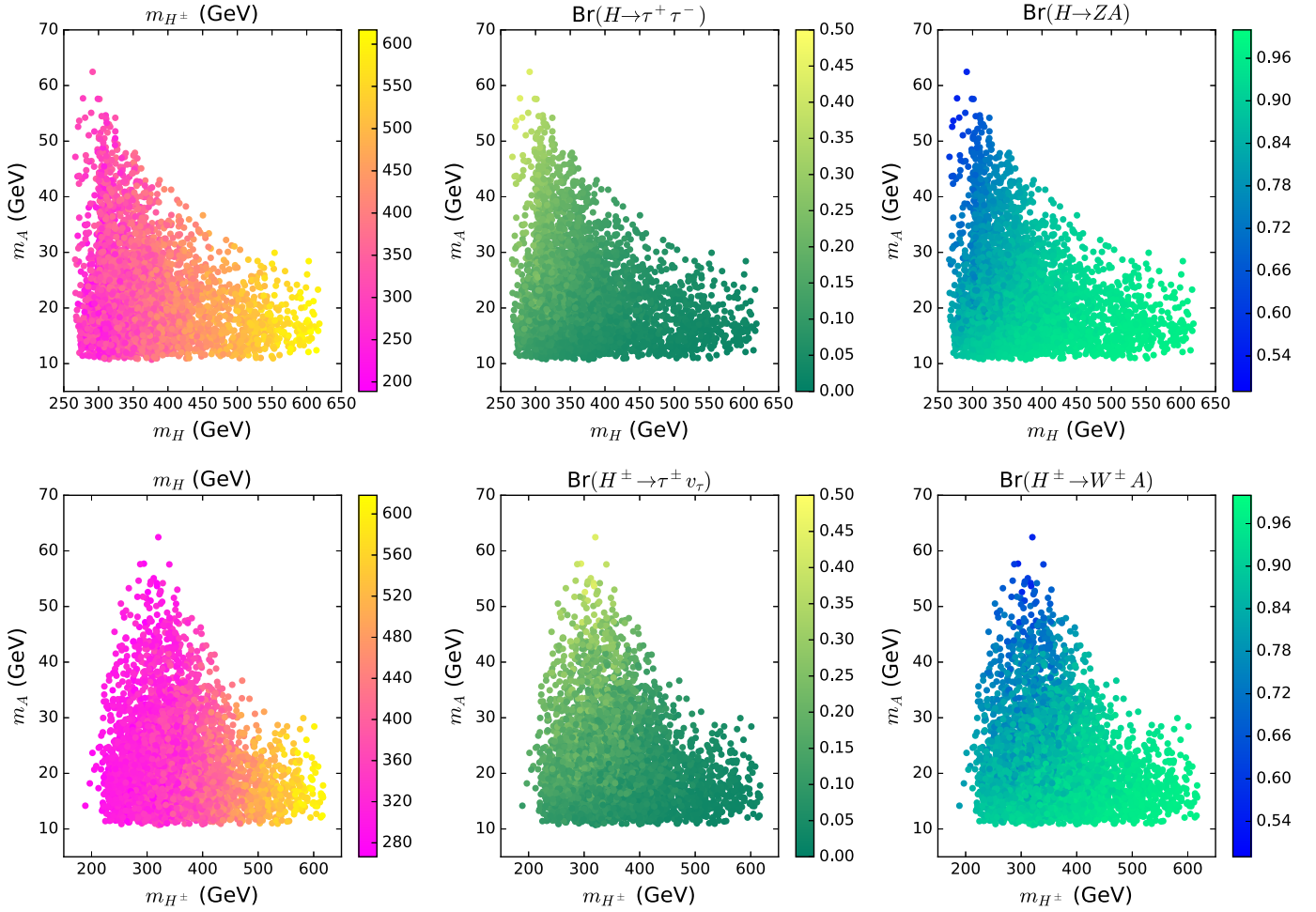
$$pp \to W^{\pm *} \to H^\pm A, \tag{25}$$

$$pp \to Z^*/\gamma^* \to HA, \tag{26}$$

$$pp \to W^{\pm *} \to H^\pm H, \tag{27}$$

$$pp \to Z^*/\gamma^* \to H^+ H^-. \tag{28}$$

In our scenario, the important decay modes of the Higgs bosons are

$$A \to \tau^+\tau^-, \ \mu^+\mu^-, \ H \to \tau^+\tau^-, \ ZA, \ H^\pm \to \tau^\pm\nu, \ W^\pm A. \tag{29}$$

Fig. 5. The samples satisfying the constraints described in Sec. 3 projected on the planes of m_H VS m_A and $m_{H\pm}$ VS m_A. The varying colors in each panel indicate the values of $m_{H\pm}$, BR($H \to \tau^+\tau^-$), BR($H \to ZA$), m_H, BR($H^\pm \to \tau^\pm v_\tau$) and BR($H^\pm \to W^\pm A$), respectively.

Here the light pseudo-scalar A indeed decays into $\tau\tau$ essentially at 100% due to the enhanced lepton Yukawa couplings by large $\tan\beta$. The other decay branch ratios and mass spectrum for the samples satisfying constraints described in Sec. 3 are presented in Fig. 5 on the planes of m_H VS m_A and $m_{H\pm}$ VS m_A. We can see from the upper panels that m_H increases from 260 GeV to 620 GeV with $m_{H\pm}$ increasing from 180 GeV to 620 GeV and the upper bounds of m_A decreasing from 65 GeV to 30 GeV. The reason is discussed in Sec. 3. As a result, the cross sections of processes in Eq. (25) and Eq. (26) are much larger than the two in Eq. (27) and Eq. (28). The middle and right panels exhibit the decay branch ratios of $H/H^\pm$ to $\tau^+\tau^-/\tau^\pm v_\tau$ and $H/H^\pm$ to gauge boson and A. With an increase of m_A, the partial widths of $H^\pm/H$ to $AW^\pm/Z$ decrease due to the suppression of phase space. The muon $g-2$ anomaly favors a large $\tan\beta$ with m_A increasing, which leads the partial widths of $H \to \tau^+\tau^-$ and $H^\pm \to \tau^\pm v_\tau$ to be enhanced since the Yukawa couplings are proportional to $\tan\beta$. Therefore, with an increase of m_A, Br($H \to AZ$) and Br($H^\pm \to W^\pm A$) decrease, and Br($H \to \tau^+\tau^-$) and Br($H^\pm \to \tau^\pm v_\tau$) increase. In conclusion, the dominated finial states generated at LHC of our samples are 3 or 4 τs with or without gauge boson from

$$pp \to W^{\pm*} \to H^\pm A \to, 3\tau + v_\tau \text{ or } 4\tau + W^\pm \quad (30)$$

$$pp \to Z^*/\gamma^* \to HA \to 4\tau \text{ or } 4\tau + Z. \quad (31)$$

In order to restrict the productions of the above processes at the LHC for our model, we perform simulations for the samples in Fig. 5 using MG5_aMC-2.4.3 [53] with PYTHIA6 [54] and Delphes-3.2.0 [55], and adopt the constraints from all the analysis for the 13 TeV LHC in version CheckMATE 2.0.7 [56]. Besides, the latest multi-lepton searches for electroweakino [57–61] implemented in Ref. [62] are also taken into consideration because of the dominated multi-τ final states in our model.

The results from CheckMATE are presented in Fig. 6 on the planes of m_H VS m_A, $m_{H\pm}$ VS m_A, and $\tan\beta$ VS m_A. The colors stand for the R values defined by [56]

$$R = \max_i \{ \frac{S_i - 1.96\Delta S_i}{S_{i,\text{Exp}}^{95}} \}, \quad (32)$$

where S_i and ΔS_i denote the number of signal events in signal region i, and $S_{i,\text{Exp}}^{95}$ is the experimentally measured 95% confidence limit on signal event in signal region i. Obviously, R > 1 means that the corresponding point is excluded at 95% confidence level by at least one search channel. We can see that the constraints from current LHC 13 TeV data shrink m_A from [10, 65] GeV to [10, 44] GeV and $\tan\beta$ from [32, 80] to [32, 60]. For the samples excluded by current 13 TeV LHC data, the strongest constraint comes from the search for electroweak production of charginos and neutralinos in multilepton final states [58]. In this analysis, 7 categories of signal region are designed for event with τ in final state, SR-C to SR-F
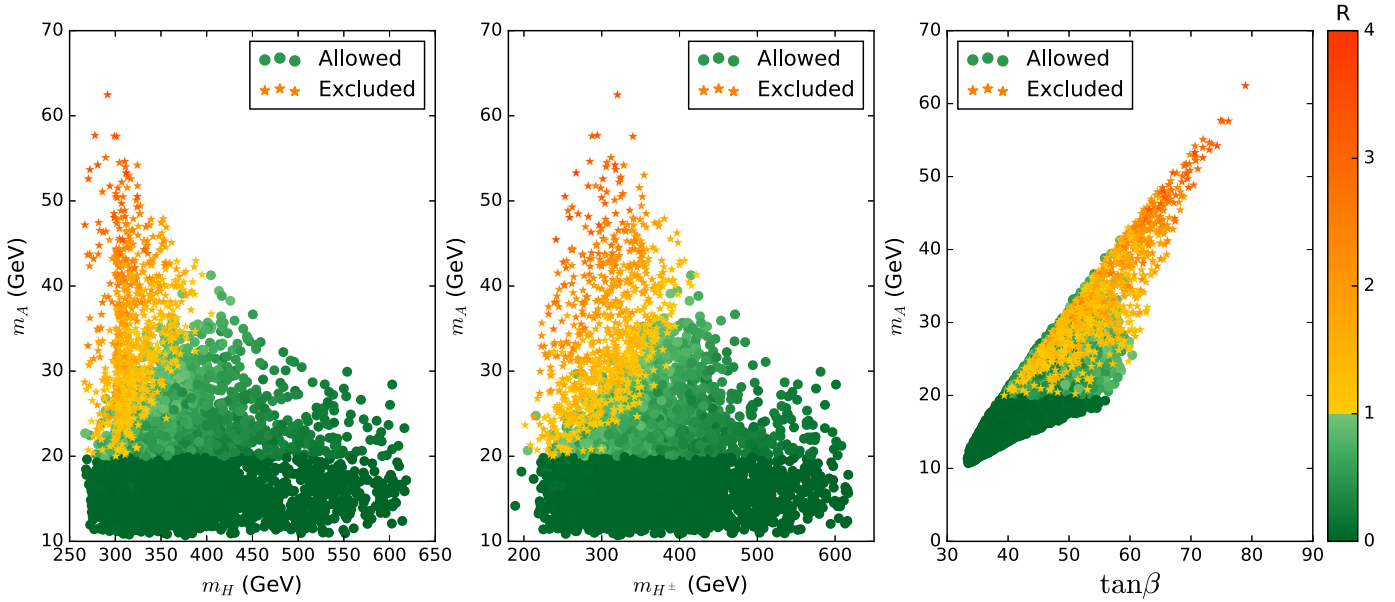
Fig. 6. The samples satisfying the constraints described in Sec. 3, projected on the planes of m_H VS m_A, $m_{H^\pm}$ VS m_A, and $\tan\beta$ VS m_A with colors indicating the R values from CheckMATE. The orange stars and green dots stand for the samples excluded and allowed by the LHC Run-2 data at 95% confidence level, respectively.

and SR-I to SR-K. The most sensitive signal region is SR-K for most of the parameter space. It requires at least two light-flavor leptons and two τ jets without b-tagged jet. The signal region is subdivided by missing energy $\not{E}_T$ to three bins, SR-K01, SR-K02, and SR-K03. The main contributions of our samples to the bins are from processes in Eq. (30) and Eq. (31) with at least two of the τs decaying hadronically.

In Fig. 6, the points with relatively larger $m_H/m_{H^\pm}$ or lower m_A can escape the direct searches. The R value decreases gently with heavier $H/H^\pm$ because of the smaller cross sections. With higher luminosity and collision energy this region can be further detected. For the light A, the τs from A in Eq. (25) to Eq. (28) decays become too soft to be distinguished at detector, while the τs from A in $H/H^\pm$ decays are collinear because of the large mass splitting between A and $H/H^\pm$. Meanwhile, the $H/H^\pm \to AZ/W^\pm$ decay modes dominate the $H/H^\pm$ decays in the low m_A region. Thus, in the region of $m_A < 20$ GeV, the acceptance of above signal region for final state of two collinear $\tau + Z/W$ boson quickly decreases.

The production processes of the extra Higgses in Eqs. (30), (31) considered by us are the same as Eqs. (26–29) of Ref. [17]. The main difference is that we implemented the constraints from 13 TeV LHC results of 36 fb^{-1} data, while Ref. [17] used the 8 TeV LHC results of 20 fb^{-1} data. Another difference is that we perform MC simulation for all survived samples instead of points on $m_A - m_H$ plane with fixed $m_{H^\pm}$ and branch ratios. In addition, the constraints of LFU in Z decay are not considered in Ref. [17]. Thus, m_H and $m_{H^\pm}$ are allowed to be large enough to satisfy the LHC searches for HA and $H^\pm A$ productions in Ref. [17]. However, the lower panels of Fig. 4 in our paper show that the limits of LFU in Z decays can impose the upper bounds of m_H and $m_{H^\pm}$ in the parameter space favored by the muon $g - 2$ anomaly, such as $m_H < 320$ GeV for $m_A = 50$ GeV. Such ranges of m_H and m_A are completely excluded by the LHC searches for HA production, and the corresponding $\tan\beta$ is also excluded.

5. The strong first-order phase transition

In this section we study the possibility to obtain a parameter space in L2HDM that can trigger a SFOPT and explain muon $g - 2$ anomaly at the same time. In order to know the strength of phase

transition in our scenario, we need to study the effective potential with thermal correction included. The thermal effective potential $V(\phi_1, \phi_2, T)$ at temperature T is composed of four parts:

$$V(\phi_1, \phi_2, T) = V^0(\phi_1, \phi_2) + V^{CW}(\phi_1, \phi_2) + V^{CT}(\phi_1, \phi_2)$$
$$+ V^T(\phi_1, \phi_2, T), \tag{33}$$

where V^0 is the tree-level potential, V^{CW} is the Coleman–Weinberg potential, V^{CT} is the counter term and V^T is the thermal correction. Concrete expressions of these terms can be found in [63].

The condition for a SFOPT is usually taken to be [64]:

$$\xi_c \equiv \frac{v_c}{T_c} \geqslant 1.0. \tag{34}$$

Here T_c is the critical temperature at which a second minimum of $V(\phi_1, \phi_2, T)$ with non-zero VEV appear, and $v_c = \sqrt{\phi_1^2 + \phi_2^2}$ is the corresponding VEV at T_c. Due to the complicated form of $V(\phi_1, \phi_2, T)$, numerical calculation is always required to analyze the geometry evolution of $V(\phi_1, \phi_2, T)$. In this work we use package BSMPT [65] to do the analysis. In BSMPT, the critical temperature T_c is determined when the minimization point $v = v_c$ at critical temperature T_c jumps to the origin $v = 0$ at a slightly higher temperature $T > T_c$.

The 4881 points allowed and excluded by the search limits of LHC in the Sec. 4 are used as input to calculate ξ_c. Out of 4881 input points, there are only 279 points that can lead to VEV jumping and a non-zero ξ_c. Because of the complicated scalar potential geometry and its dependence on T, it is hard to find obvious relation between our zero temperature inputs and the strength of phase transition. While in [66,67], it is pointed out that the depth of minimum point at zero temperature has a strong correlation with phase transition strength. If the zero temperature vacuum energy in a model (noted as $\mathcal{F}_0$) is higher than the zero temperature vacuum energy in the SM (noted as $\mathcal{F}_0^{SM}$), then the phase transition of this model tends to be SFOPT. A $\mathcal{F}_0$ under $\mathcal{F}_0^{SM}$ can also trigger a first order phase transition, but with a lower probability and a lower phase transition strength. The difference between
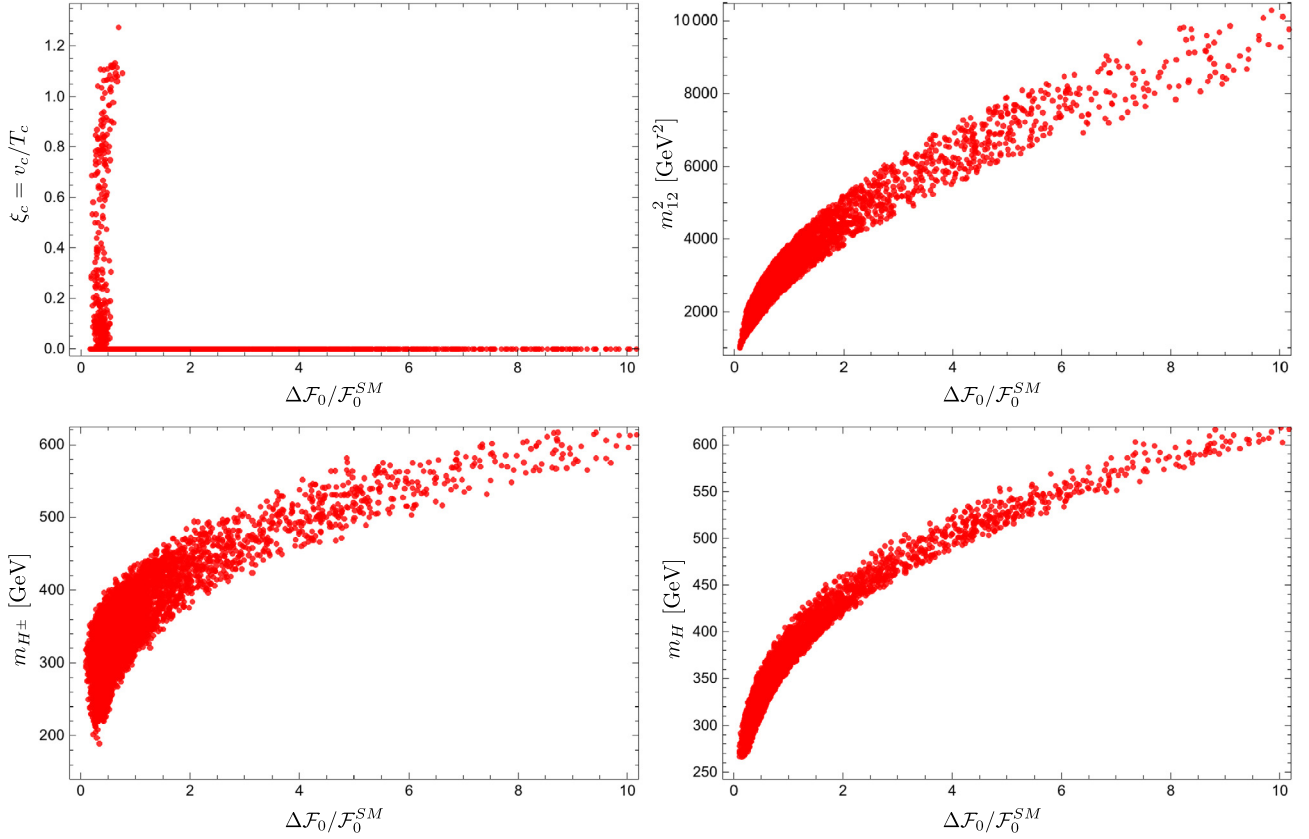
Fig. 7. Upper-left: relationship between $\Delta\mathcal{F}_0/\mathcal{F}_0^{SM}$ and ξ_c. Points with $\xi_c = 0$ do not have a first order phase transition. Relationships between $\Delta\mathcal{F}_0/\mathcal{F}_0^{SM}$ and m_{12}^2 (upper-right), $\Delta\mathcal{F}_0/\mathcal{F}_0^{SM}$ and $m_{H^\pm}$ (lower-left), and $\Delta\mathcal{F}_0/\mathcal{F}_0^{SM}$ and m_H (lower-right).
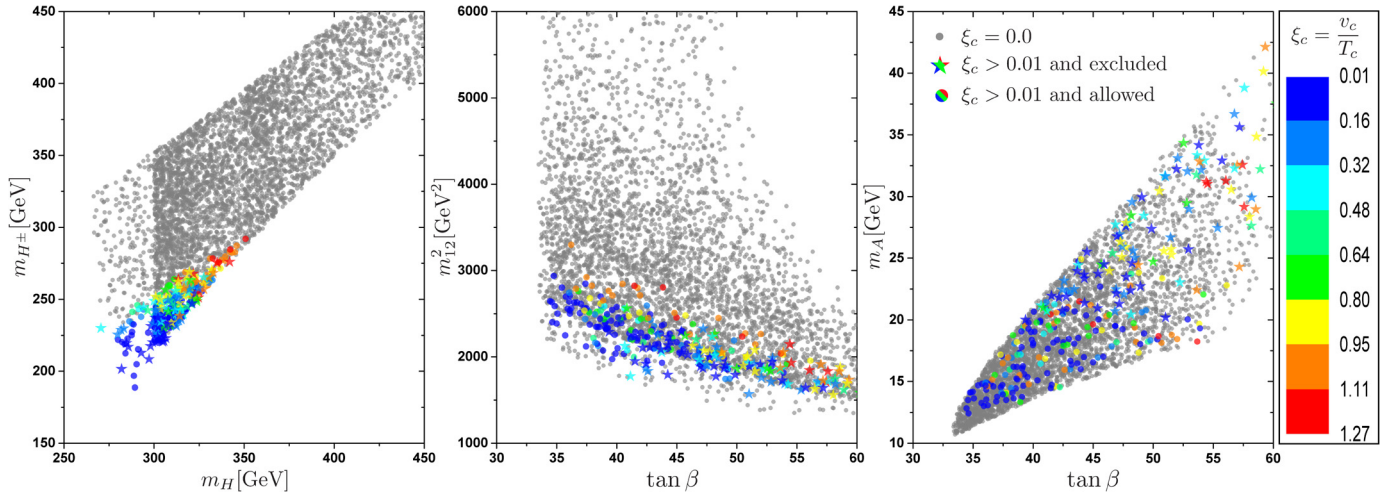
Fig. 8. m_H VS $m_{H^\pm}$ plane (left panel), $\tan\beta$ VS m_{12}^2 (middle) and $\tan\beta$ VS m_A (right) with color mapped by ξ_c. Grey points do not have a SFOPT. Colored spots are allowed points under current limits, and colored stars are excluded by the LHC direct search.

$\mathcal{F}_0$ and $\mathcal{F}_0^{SM}$ at one-loop level in 2HDM with alignment limit ($\sin(\beta - \alpha) \to 1$) has been given in [67]:

$$\Delta\mathcal{F}_0 \equiv \mathcal{F}_0 - \mathcal{F}_0^{SM}$$

$$= \frac{1}{64\pi^2}\left[(m_h^2 - 2M^2)^2\left(\frac{3}{2} + \frac{1}{2}\log\left[\frac{4m_A m_H m_{H^\pm}}{(m_h^2 - 2M^2)^2}\right]\right)\right]$$

$$+ \frac{1}{2}(m_A^4 + m_H^4 + 2m_{H^\pm}^4)$$

$$+ (m_h^2 - 2M^2)(m_A^2 + m_H^2 + 2m_{H^\pm}^2) \,. \tag{35}$$

Here $M^2 = m_{12}^2(\tan\beta + \tan\beta^{-1})$. The SM one-loop vacuum energy $\mathcal{F}_0^{SM} \approx -1.25 \times 10^8$ GeV^4.

In Fig. 7 we show the relationship between $\Delta\mathcal{F}_0/\mathcal{F}_0^{SM}$ and ξ_c. The first order phase transition can only happen in the region with $\Delta\mathcal{F}_0/\mathcal{F}_0^{SM} < 1.0$. This is consistent with the relationship found in [67]. Here we need to emphasize that even there is a strong correlation between $\Delta\mathcal{F}_0/\mathcal{F}_0^{SM}$ and phase transition, it doesn't mean that the phase transition is decided by $\Delta\mathcal{F}_0/\mathcal{F}_0^{SM}$ solely. In

Table 2
Several benchmark points achieving the SFOPT.

Benchmark points	A	B	C	D
$\sin(\beta - \alpha)$	0.999	0.9989	0.9992	0.9987
$\tan\beta$	48.57	46.09	53.66	41.46
m_h (GeV)	125.0	125.0	125.0	125.0
m_H (GeV)	314.96	322.95	330.88	342.27
m_A (GeV)	18.22	20.3	18.24	20.45
$m_{H^\pm}$ (GeV)	253.27	259.89	264.59	284.7
m_{12}^2 (GeV^2)	2041.32	2261.78	2039.42	2823.33
$\xi_c = v_c/T_c$	1.015	1.066	1.117	1.132

the region with $\Delta\mathcal{F}_0/\mathcal{F}_0^{SM} < 1.0$, the probability for $\xi_c > 0.0$ and $\xi_c > 1.0$ are 8.3% and 0.8%. Thus in order to get SFOPT, a certain level of parameter fine tuning is required. In our parameter space, $m_{H^\pm}$, m_H, and m_{12}^2 are closely related to $\Delta\mathcal{F}_0/\mathcal{F}_0^{SM}$, see plots in Fig. 7. While $\tan\beta$ and m_A are not so relevant to phase transition in our scenario. Furthermore, in Fig. 8 we project all the points on the planes of m_H VS $m_{H^\pm}$, $\tan\beta$ VS m_{12}^2, and $\tan\beta$ VS m_A with color mapped by ξ_c. It can be seen that $\xi_c > 0.0$ and $\xi_c > 1.0$ constrain the planes of m_H VS $m_{H^\pm}$ and m_{12}^2 VS $\tan\beta$ to very narrow regions, but the phase transition is not sensitive to $\tan\beta$ and m_A. The points with $\xi_c > 0.0$ and $m_A > 25$ GeV are excluded by the direct searches limits of LHC.

To conclude this section, SFOPT and the explanation of muon $g - 2$ in L2HDM can happen in a small subset of 2HDM parameter space, where 14 GeV $< m_A < 25$ GeV, 310 GeV $< m_H < 355$ GeV, and 250 GeV $< m_{H^\pm} < 295$ GeV. We list detailed information of several benchmark points achieving the SFOPT and explaining the muon $g - 2$ anomaly in Table 2.

6. Conclusion

The L2HDM can provide a simple explanation for the muon $g - 2$ anomaly. We performed a scan over the parameter space of L2HDM to identify the ranges in favor of the muon $g - 2$ explanation after imposing various relevant theoretical and experimental constraints, especially the direct search limits from LHC and a SFOPT in the early universe. We found that the muon $g - 2$ anomaly can be accommodated in the region of $32 < \tan\beta < 80$, 10 GeV $< m_A < 65$ GeV, 260 GeV $< m_H < 620$ GeV and 180 GeV $< m_{H^\pm} < 620$ GeV after imposing the joint constraints from the theory, the precision electroweak data, the 125 GeV Higgs signal data, the LFU in τ and Z decays, and the measurement of Br($B_s \to \mu^+\mu^-$). The direct search limits from the LHC can give stringent constraints on m_A and $\tan\beta$ for small m_H and $m_{H^\pm}$: 10 GeV $< m_A < 44$ GeV and $32 < \tan\beta < 60$. The direct search limits from the $h \to AA$ channels at the LHC can impose stringent upper limits on Br($h \to AA$). Finally, we found that a SFOPT can be achievable in the region of 14 GeV $< m_A < 25$ GeV, 310 GeV $< m_H < 355$ GeV, and 250 GeV $< m_{H^\pm} < 295$ GeV while the muon $g - 2$ anomaly is accommodated.

Acknowledgement

References

[1] H.N. Brown, et al., Muon g-2 Collaboration, Phys. Rev. Lett. 86 (2001) 2227.
[2] G.W. Bennett, et al., Muon g-2 Collaboration, Phys. Rev. D 73 (2006) 072003.
[3] F. Jegerlehner, A. Nyffeler, Phys. Rep. 477 (2009) 1.
[4] G. Colangelo, M. Hoferichter, A. Nyffeler, M. Passera, P. Stoffer, Phys. Lett. B 735 (2014) 90.
[5] A. Kurz, T. Liu, P. Marquard, M. Steinhauser, Phys. Lett. B 734 (2014) 144.
[6] A. Dedes, H.E. Haber, J. High Energy Phys. 0105 (2001) 006.
[7] D. Chang, W.-F. Chang, C.-H. Chou, W.-Y. Keung, Phys. Rev. D 63 (2001) 091301.
[8] K.M. Cheung, C.H. Chou, O.C.W. Kong, Phys. Rev. D 64 (2001) 111301.
[9] F. Larios, G. Tavares-Velasco, C.P. Yuan, Phys. Rev. D 64 (2001) 055004.
[10] K. Cheung, O.C.W. Kong, Phys. Rev. D 68 (2003) 053003.
[11] J. Cao, P. Wan, L. Wu, J.M. Yang, Phys. Rev. D 80 (2009) 071701.
[12] J.S. Lee, A. Pilaftsis, Phys. Rev. D 86 (2012) 035004.
[13] M. Krawczyk, arXiv:hep-ph/0103223.
[14] A. Broggio, E.J. Chun, M. Passera, K.M. Patel, S.K. Vempati, J. High Energy Phys. 1411 (2014) 058.
[15] L. Wang, X.F. Han, J. High Energy Phys. 05 (2015) 039.
[16] T. Abe, R. Sato, K. Yagyu, J. High Energy Phys. 1507 (2015) 064.
[17] E.J. Chun, Z. Kang, M. Takeuchi, Y.-L. Tsai, J. High Energy Phys. 1511 (2015) 099.
[18] T. Han, S.K. Kang, J. Sayre, J. High Energy Phys. 1602 (2016) 097.
[19] V. Ilisie, J. High Energy Phys. 1504 (2015) 077.
[20] A. Cherchiglia, P. Kneschke, D. Stockinger, H. Stockinger-Kim, J. High Energy Phys. 1701 (2017) 007.
[21] X. Liu, L. Bian, X.-Q. Li, J. Shu, Nucl. Phys. B 909 (2016) 507–524.
[22] E.J. Chun, J. Kim, J. High Energy Phys. 1607 (2016) 110.
[23] X.-F. Han, L. Wang, J.M. Yang, Phys. Lett. B 757 (2016) 537–547.
[24] B. Batell, N. Lange, D. McKeen, M. Pospelov, A. Ritz, Phys. Rev. D 95 (2017) 075003.
[25] A. Cherchiglia, P. Kneschke, D. Stockinger, H. Stockinger-Kim, J. High Energy Phys. 1701 (2017) 007.
[26] A. Cherchiglia, D. Stöckinger, H. Stöckinger-Kim, Phys. Rev. D 98 (2018) 035001.
[27] S.-P. Li, X.-Q. Li, Y.-D. Yang, arXiv:1808.02424.
[28] E.J. Chun, S. Dwivedi, T. Mondal, B. Mukhopadhyaya, Phys. Lett. B 774 (2017) 20–25.
[29] E.J. Chun, S. Dwivedi, T. Mondal, B. Mukhopadhyaya, S.K. Rai, arXiv:1807.05379.
[30] A. Crivellin, J. Heeck, P. Stoffer, Phys. Rev. Lett. 116 (2016) 081801.
[31] M. Lindner, M. Platscher, F.S. Queiroz, Phys. Rep. 731 (2018) 1–82.
[32] A.I. Bochkarev, S.V. Kuzmin, M.E. Shaposhnikov, Phys. Lett. B 244 (1990) 275;
G.C. Dorsch, S.J. Huber, J.M. No, J. High Energy Phys. 1310 (2013) 029;
P. Basler, M. Krause, M. Muhlleitner, J. Wittbrodt, A. Wlotzka, J. High Energy Phys. 1702 (2017) 121;
G.C. Dorsch, S.J. Huber, K. Mimasu, J.M. No, Phys. Rev. Lett. 113 (2014) 211802;
K. Fuyuto, E. Senaha, Phys. Lett. B 747 (2015) 152;
C.W. Chiang, K. Fuyuto, E. Senaha, Phys. Lett. B 762 (2016) 315;
J. Bernon, L. Bian, Y. Jiang, J. High Energy Phys. 1805 (2018) 151;
F.P. Huang, J.-H. Yu, arXiv:1704.04201;
C.-H. Cao, F.P. Huang, K.-P. Xie, X. Zhang, Chin. Phys. C 42 (2018) 023103.
[33] J.M. Cline, K. Kainulainen, M. Trott, J. High Energy Phys. 1111 (2011) 089.
[34] A.D. Sakharov, Pis'ma Zh. Eksp. Teor. Fiz. 5 (1967) 32;
A.D. Sakharov, JETP Lett. 5 (1967) 24;
A.D. Sakharov, Sov. Phys. Usp. 34 (5) (1991) 392;
A.D. Sakharov, Usp. Fiz. Nauk 161 (5) (1991) 61.
[35] M. Kamionkowski, A. Kosowsky, M.S. Turner, Phys. Rev. D 49 (1994) 2837.
[36] C. Caprini, et al., J. Cosmol. Astropart. Phys. 1604 (04) (2016) 001.
[37] R.A. Battye, G.D. Brawn, A. Pilaftsis, J. High Energy Phys. 1108 (2011) 020.
[38] V.D. Barger, J.L. Hewett, R.J.N. Phillips, Phys. Rev. D 41 (1990) 3421.
[39] A.G. Akeroyd, W.J. Stirling, Nucl. Phys. B 447 (1995) 3.
[40] D. Eriksson, J. Rathsman, O. Stål, Comput. Phys. Commun. 181 (2010) 189.
[41] ATLAS and CMS Collaborations, J. High Energy Phys. 1608 (2016) 045.
[42] Y. Amhis, et al., Heavy Flavor Averaging Group (HFAG) Collaboration, arXiv:1412.7515.
[43] S. Schael, et al., ALEPH and DELPHI and L3 and OPAL and SLD and LEP Electroweak Working Group and SLD Electroweak Group and SLD Heavy Flavour Group Collaborations, Phys. Rep. 427 (2006) 257.
[44] G. Bennett, et al., Muon G-2 Collaboration, Phys. Rev. D 73 (2006) 072003.
[45] F. Jegerlehner, A. Nyffeler, Phys. Rep. 477 (2009) 1–110.
[46] X.-Q. Li, J. Lu, A. Pich, J. High Energy Phys. 1406 (2014) 022.
[47] R. Aaij, et al., LHCb Collaboration, Phys. Rev. Lett. 118 (2017) 191801.
[48] ATLAS Collaboration, Search for Higgs bosons decaying to aa in the $\mu\mu\tau\tau$ final state in pp collisions at $\sqrt{s} = 8$ TeV with the ATLAS experiment, Phys. Rev. D 92 (2015) 052002.
[49] CMS Collaboration, Search for light bosons in decays of the 125 GeV Higgs boson in proton–proton collisions at $\sqrt{s} = 8$ TeV, J. High Energy Phys. 1710 (2017) 076.

[50] P. Bechtle, O. Brein, S. Heinemeyer, G. Weiglein, K.E. Williams, Comput. Phys. Commun. 181 (2010) 138–167.

[51] P. Bechtle, O. Brein, S. Heinemeyer, O. Stål, T. Stefaniak, G. Weiglein, K.E. Williams, Eur. Phys. J. C 74 (2014) 2693.

[52] J. Bernon, J.F. Gunion, Y. Jiang, Phys. Rev. D 91 (2015) 075019.

[53] J. Alwall, et al., J. High Energy Phys. 1407 (2014) 079.

[54] P. Torrielli, S. Frixione, J. High Energy Phys. 1004 (2010) 110.

[55] J. de Favereau, et al., DELPHES 3 Collaboration, J. High Energy Phys. 1402 (2014) 057.

[56] D. Dercks, N. Desai, J.S. Kim, K. Rolbiecki, J. Tattersall, T. Weber, Comput. Phys. Commun. 221 (2017) 383.

[57] A.M. Sirunyan, et al., CMS Collaboration, J. High Energy Phys. 1803 (2018) 160.

[58] A.M. Sirunyan, et al., CMS Collaboration, J. High Energy Phys. 1803 (2018) 166.

[59] A.M. Sirunyan, et al., CMS Collaboration, J. High Energy Phys. 1803 (2018) 076.

[60] A.M. Sirunyan, et al., CMS Collaboration, J. High Energy Phys. 1711 (2017) 029.

[61] M. Aaboud, et al., ATLAS Collaboration, Eur. Phys. J. C 78 (2018) 154.

[62] G. Pozzo, Y. Zhang, arXiv:1807.01476.

[63] S.R. Coleman, E.J. Weinberg, Phys. Rev. D 7 (1973) 1888;
J.M. Cline, K. Kainulainen, M. Trott, J. High Energy Phys. 1111 (2011) 089;
L. Dolan, R. Jackiw, Phys. Rev. D 9 (1974) 3320;
M. Quiros, arXiv:hep-ph/9901312;
P.B. Arnold, O. Espinosa, Phys. Rev. D 47 (1993) 3546, Erratum: Phys. Rev. D 50 (1994) 6662;
P. Basler, M. Krause, M. Muhlleitner, J. Wittbrodt, A. Wlotzka, J. High Energy Phys. 1702 (2017) 121.

[64] M. Quiros, Helv. Phys. Acta 67 (1994) 451;
G.D. Moore, Phys. Rev. D 59 (1999) 014503.

[65] P. Basler, M. Muhlleitner, arXiv:1803.02846.

[66] W. Huang, Z. Kang, J. Shu, P. Wu, J.M. Yang, Phys. Rev. D 91 (2) (2015) 025006, https://doi.org/10.1103/PhysRevD.91.025006, arXiv:1405.1152 [hep-ph];
C.P.D. Harman, S.J. Huber, J. High Energy Phys. 1606 (2016) 005, https://doi.org/10.1007/JHEP06(2016)005, arXiv:1512.05611 [hep-ph].

[67] G.C. Dorsch, S.J. Huber, K. Mimasu, J.M. No, J. High Energy Phys. 1712 (2017) 086.